Frequency-Domain Channel Characteristics of Intelligent Reflecting Surface Assisted Visible Light Communication

Cheng Chen, Shenjie Huang, Hanaa Abumarshoud, *Senior Member, IEEE*, Iman Tavakkolnia, *Member, IEEE*, Majid Safari, *Senior Member, IEEE* and Harald Haas, *Fellow, IEEE*

***Abstract*—Deploying an intelligent reflecting surface (IRS) array in visible light communication (VLC) systems forms additional light propagation paths, thereby enhancing the optical wireless channel. This improves the aggregated received signal strength, but on the other hand, it also introduces time delays between received signals via different paths. In this paper, the impact of IRS-induced time delay on the VLC channel characteristics in the frequency-domain is investigated for the first time in the open literature. The considered issue is experimentally validated. In addition, the influence of IRS-induced time delay in practical scenarios considering users with fixed and random positions has also been evaluated. It is demonstrated that an IRS array can consistently improve the performance of narrowband VLC systems. In wideband VLC systems, the performance gain is considerable when the reflected channel via the IRS array is significantly greater than the line-of-sight (LoS) channel. However, when the path losses for both reflected and LoS signals are similar, the communication performance does not show noticeable improvement compared to the case with only the LoS path.**

***Index Terms*—Visible light communication, optical wireless communication, intelligent reflecting surface, optical wireless channel.**

I. Introduction

The future 6th-generation (6G) is envisioned as a powerful wireless network with global coverage, all spectrum usage and embedded intelligence, which can provide super-high data rates to a massive number of users and devices [1]. Visible light communication (VLC) and light-fidelity (LiFi) use optical spectrum to provide multi-Gbps wireless transmission speed. As potential enablers for 6G and beyond networks, VLC and LiFi systems offer multiple advantages in terms of security, data density and lighting functionalities [2], [3]. In conventional radio frequency (RF) wireless communications, the concept of intelligent reflecting surface (IRS) has been proposed to improve the wireless link performance in terms of spectral efficiency, multiple access and security [4], [5]. The basic idea is to deploy an adaptive reflective unit to direct the incoming signal to the targeted mobile user. By tuning the reflection coefficients, the wireless channel can be manipulated to achieve the desired performance.

Motivated by the latest advances in IRS-aided RF wireless communication, optical IRSs and smart optics have been proposed to assist various optical wireless communication (OWC) systems [6]–[10]. Similar to their RF counterparts, optical IRS arrays can effectively increase the received signal power, thereby greatly improving system reliability or spectral efficiency. Furthermore, optical IRSs are particularly useful for combating link blockage in OWC systems, which is a more critical issue compared to RF wireless systems. so that the received signal strength is enhanced and some link blockage issues can be avoided. Most VLC systems use intensity modulation (IM) with direct detection (DD). In conjunction with the large detection area relative to the wavelength in the optical region, small scale fading in VLC is negligible [11]. Therefore, multiple received optical signals via different paths can be combined constructively without stringent phase control. This feature makes the operation of IRSs in VLC fundamentally different from that in RF wireless systems. In IRS-assisted RF wireless systems, tuning the reflection matrix with optimal phase is important for achieving the highest gain [4]. In IRS-assisted VLC systems, it is vital to control the reflection units to bounce the optical signal to the desired target direction [7].

Potential benefits, techniques and challenges for the use of IRS in LiFi networks have been comprehensively discussed in [8]. An analytical framework to study the performance of two types of IRSs is presented in [7], where the adaptive metasurface array controls the reflection direction by manipulating the light phase gradient, and the mirror array controls the reflection direction by changing the mechanical orientations of mirror elements. In [12], optimisation problems have been formulated to maximise the achievable data rate by the IRS-assisted VLC systems, which demonstrate the capability of IRS to improve the VLC data rate. IRS has been proposed to improve the multiple access capability [13] and physical layer security in VLC systems [14], [15].

Despite little concern about small-scale fading in OWC due to photodiode (PD) spatial averaging, the effects of combining multipath with different delays still cause inter-symbol interference, which leads to a non-flat channel in

Cheng Chen, Iman Tavakkolnia and Harald Haas are with the Department of Electrical and Electrical Engineering, the University of Strathclyde, Glasgow, Scotland, UK, e-mail: {cheng.chen, i.tavakkolnia, h.haas}@strath.ac.uk.

Hanaa Abumarshoud is with the Autonomous Systems & Connectivity Division, James Watt School of Engineering, University of Glasgow, Glasgow, Scotland, UK, e-mail: hanaa.abumarshoud@glasgow.ac.uk.

Shenjie Huang and Majid Safari are with the Institute for Digital Communications, School of Engineering, University of Edinburgh, Edinburgh, Scotland, UK, e-mail: {shenjie.huang, majid.safari}@ed.ac.uk

The authors acknowledge financial support from the Engineering and Physical Sciences Research Council (EPSRC) under grant EP/S016570/1 'Terabit Bidirectional Multi-User Optical Wireless System (TOWS) for 6G LiFi'. *(Corresponding authors: Shenjie Huang)*

frequency domain [11]. In most existing research on OWC with IRS, the IRS-induced time delay has been omitted and the same time of arrival is assumed for all multipath components [7], [12]–[14]. Consequently, the performance gains introduced by optical IRS in these studies are likely to be overestimated. VLC channel characteristics with non-line-of-sight (NLoS) propagation paths due to reflections have been considered in numerous research works [16], [17]. However, these studies primarily focus on reflections caused by indoor internal surfaces. In contrast, the channel delay profile caused by IRS exhibits significantly different characteristics. A comprehensive tapped-delay line channel model of IRS-assisted VLC systems considering various cases and assumptions has been proposed in [18], where the time delay spread caused by the reflected paths via IRS has been evaluated and characterised. The link signal-to-noise ratio (SNR) in a communication system is determined by channel responses over the modulation bandwidth. Therefore, it is important to understand the frequency-domain channel characteristics of the IRS-assisted VLC systems. In this paper, we focus on investigating the frequency-domain channel characteristics of IRS-assisted VLC systems considering the IRS-induced time delay. The corresponding impact on the communication performance has also been studied. The contributions of this work are the following:

- The characteristics of frequency selective channel due to IRS-induced time delay is investigated and further validated by experiments. A single IRS element model is used to simplify the performance analysis and experimental validation.
- The impact of key quantities, such as IRS to line-of-sight (LoS) path loss ratio and relative time delay, on the IRS assisted VLC system is investigated. It has been found that the IRS array improves the VLC system performance when it is a narrowband system or when the strength of the reflected channel via the IRS array is significantly greater than the LoS channel. When the strength of the reflected channel is similar to the LoS channel in a wideband VLC system, the use of IRS array leads to similar or even worse performance compared to the case with LoS channel only.
- The achievable rate analysis of IRS-assisted VLC systems with direct current-biased optical (DCO)-orthogonal frequency division multiplexing (OFDM) is presented. In particular, a closed-form expression for the achievable rate with uniform power allocation and a single element IRS model is derived.
- The communication performance in terms of SNR, bit error ratio (BER) and achievable rate of IRS-assisted VLC systems under the time delay effects are evaluated. In addition, the performance statistics for random user position and orientations are evaluated. The finding implies that the activation of the IRS array should be channel-dependent or a gain control mechanism may be required.

The aim of this study is to demonstrate the importance of considering the IRS-induced time delay issue and to comprehend the features of the IRS-assisted channel in an indoor VLC system.

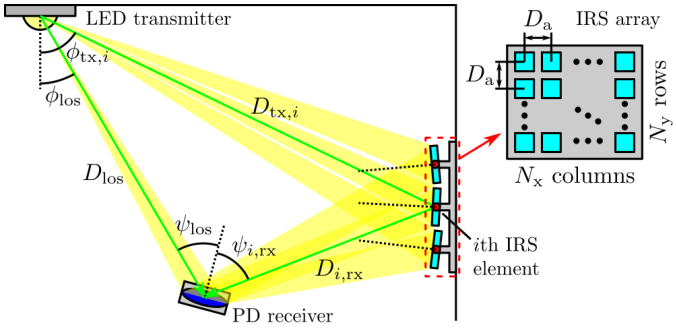

Figure 1: Channel model for VLC with assistance of an IRS array.

The remainder of this paper is organised as follows: Section II introduces the considered IRS-assisted VLC system model. Section III presents a simplified single element IRS model including its experimental validation and investigation on the impacts of key metrics. Section IV presents the achievable rate analysis of IRS-assisted VLC systems with DCO-OFDM. Section V presents the communication performance simulation results in practical indoor scenarios. A discussion on the potential future research directions with IRS-induced time delay is provided in Section VI. Finally, Section VII concludes this paper.

II. System Model

The considered VLC system is deployed in an indoor environment and includes the light propagation via the LoS path and the light propagations via the IRS elements.

A. Channel via the LoS path

The LoS path loss can be described by the following expression based on a Lambertian radiation pattern as [11]:

$$G_{\mathrm{los}} = \frac{(m+1)A_{\mathrm{d}}G_{\mathrm{v}}}{2\pi D_{\mathrm{los}}^2}\cos^m(\phi_{\mathrm{los}})\cos(\psi_{\mathrm{los}}), \qquad (1)$$

where A_{d} is the detector area, D_{los} is the euclidean distance between the transmitter and the receiver, ϕ_{los} is the LoS channel light radiant angle from the light emitting diode (LED), ψ_{los} is the LoS channel light incident angle to the PD, m is the Lambertian order which is related the LED half-power semiangle $\phi_{1/2}$ by $m = -1/\log_2(\cos\phi_{1/2})$ and G_{v} is defined as a visibility factor which equals zero if either ϕ_{los} is greater than 90°or ψ_{los} is greater than the field-of-view (FoV) of the receiver ψ_{fov}. Otherwise, it equals one.

B. Channel via IRS array

Apart from the LoS channel, reflected channels can be established by deploying an IRS array, as shown in Fig. 1. In this study, an adaptive mirror array is considered due to its simplicity, but the methodology and the characterisation of time delay impact is applicable to other types of IRS, such as metasurface-based IRS array, as well. The considered IRS array has $N_{\mathrm{irs}} = N_{\mathrm{x}} \times N_{\mathrm{y}}$ tunable mirror elements with an inter-element separation of D_{a}. We assume that each

IRS element is composed of a high-conductivity material featuring a smooth surface relative to visible light wavelengths. This design ensures that each IRS element exhibits near-perfect specular reflection with high reflectivity (approaching unity) and maintains equal incident and reflection angles for the incoming light. Additionally, each IRS element can automatically adjust its orientation via two rotational degrees of freedom to reflect the incident light from the LED to the desired direction where the PD is located [7]. This function makes the reflected channel to be independent of the incident and reflection angles concerning an IRS element. The rotation angles of the IRS elements are in the range of $[-\pi/2, \pi/2]$, which are sufficient to cover any user in the room. In addition, the point source case introduced in [7] is used for simplicity, which assumes a sufficiently small LED emission area relative to the length of reflection propagation path. In practice, there could be several practical issues surrounding the use of the IRS array, such as the mechanical limitation to the range of rotation angles and acquiring the channel state information (CSI) for IRS direction control. In addition, the reflected light path via one IRS element could be blocked by an adjacent IRS element at large rotation angles. There is also a special case with a large source and a small IRS reflector. Some of these practical concerns were investigated in [7]. However, this work focuses on the impacts of IRS-induced time delay and these practical issues are out of the scope of this work. The path loss via the ith IRS element with a point source assumption can be calculated by [7]:

$$G_i = \frac{\rho(m+1)A_{\mathrm{d}}G_{\mathrm{v}}}{2\pi\left(D_{\mathrm{tx},i}+D_{i,\mathrm{rx}}\right)^2}\cos^m(\phi_{\mathrm{tx},i})\cos(\psi_{i,\mathrm{rx}}), \quad (2)$$

where ρ is the mirror reflectivity, $D_{\mathrm{tx},i}$ is the distance between the LED and the ith IRS element, $D_{i,\mathrm{rx}}$ is the distance between the ith IRS element and the PD, $\phi_{\mathrm{tx},i}$ is the light radiant angle from the LED to the ith IRS element and $\psi_{i,\mathrm{rx}}$ is the light incident angle from the ith IRS element to the PD. In this study, the light propagation time delay is considered. In conjunction with the LoS channel, the VLC channel impulse response (CIR) can be calculated as:

$$h(t) = \mathbf{1}_{\mathrm{los}}G_{\mathrm{los}}\delta(t-\tau_{\mathrm{los}}) + \mathbf{1}_{\mathrm{irs}}\sum_{i=1}^{N_{\mathrm{irs}}}G_i\delta(t-\tau_i), \quad (3)$$

where $\delta(u)$ is the Dirac delta function and the terms $\tau_{\mathrm{los}} = D_{\mathrm{los}}/c$ and $\tau_i = \left(D_{\mathrm{tx},i}+D_{i,\mathrm{rx}}\right)/c$ are the signal propagation delays via the LoS path and the ith IRS element, respectively. Note that c is the speed of light. In addition, $\mathbf{1}_{\mathrm{los}}$ is an indicator function which equals unity if the LoS path exists and equals zero otherwise. The indicator function $\mathbf{1}_{\mathrm{irs}}$ is defined similarly, which is determined by the existence of reflected paths via the IRS array. The corresponding channel frequency response (CFR) can be found as:

$$H(f) = \mathbf{1}_{\mathrm{los}}G_{\mathrm{los}}\mathrm{e}^{-2\pi jf\tau_{\mathrm{los}}} + \mathbf{1}_{\mathrm{irs}}\sum_{i=1}^{N_{\mathrm{irs}}}G_i\mathrm{e}^{-2\pi jf\tau_i}, \quad (4)$$

which is a superposition of multiple complex exponential components.

C. PAM-SCFDE transmission

The considered VLC system uses pulse amplitude modulation (PAM)-single carrier frequency domain equalisation (SCFDE) to demonstrates the resultant communication performance. PAM-SCFDE achieves a low peak-to-average power ratio (PAPR) and can use the single-tap frequency domain equalisation [19]. The unipolar SNR with zero-forcing (ZF) equalisation can be calculated as [20]:

$$\gamma = \frac{4P_{\mathrm{opt}}^2(2M-1)KT_{\mathrm{s}}R_{\mathrm{pd}}^2}{3(M-1)N_0\sum_{k=0}^{K-1}\left|H\left(\frac{k}{KT_{\mathrm{s}}}\right)\right|^{-2}}, \quad (5)$$

where P_{opt} is the LED optical power, M is the PAM modulation order, K is the fast Fourier transform (FFT) size, T_{s} is the symbol period, R_{pd} is the PD responsivity, $\left|H\left(\frac{k}{KT_{\mathrm{s}}}\right)\right|$ can be evaluated by (4) with $f = \frac{k}{KT_{\mathrm{s}}}$ and N_0 is the noise power spectral density (PSD) which is defined as:

$$N_0 = \frac{4\mathcal{K}_{\mathrm{b}}\mathcal{T}_{\mathrm{a}}}{R_{\mathrm{L}}} + 2qR_{\mathrm{pd}}P_{\mathrm{opt,rx}}, \quad (6)$$

where $\mathcal{K}_{\mathrm{b}}$ is defined as the Boltzmann's constant, $\mathcal{T}_{\mathrm{a}}$ is the absolute temperature, q is electric charge, R_{L} is the receiver load resistance and $P_{\mathrm{opt,rx}}$ is the optical power detected by the PD. Note that more advanced equalisation techniques can be used to marginally improve the SNR, but the findings in this paper still hold. Then, the following lower bound can be used to evaluate the BER [21]:

$$\mathcal{P}_{\mathrm{b}} \geq \frac{2(M-1)}{M\log_2 M}\mathcal{Q}\left(\sqrt{\frac{3\gamma}{2(2M^2-3M+1)}}\right), \quad (7)$$

where $\mathcal{Q}(u)$ is the standard Q-function.

III. Single IRS element model analysis

To investigate the channel characteristics with the assistance of the IRS array considering the time delay, we consider a simplified case of the channel model introduced in Section II, where there is only one IRS element. The simplified channel model CFR can be written as:

$$H(f) = \mathbf{1}_{\mathrm{los}}G_{\mathrm{los}}\mathrm{e}^{-2\pi jf\tau_{\mathrm{los}}} + \mathbf{1}_{\mathrm{irs}}G_{\mathrm{irs}}\mathrm{e}^{-2\pi jf\tau_{\mathrm{irs}}}. \quad (8)$$

The values of the channel gain $|H(f)|^2$ at different frequencies f over the signalling bandwidth is important, because they determine the received SNR, as shown in (5). In the case with the LoS path only or the IRS path only, either $\mathbf{1}_{\mathrm{los}}$ or $\mathbf{1}_{\mathrm{irs}}$ equals zero so that only one term remains in (8). Therefore, the channel gain is simply square of the corresponding path loss G_{los}^2 or G_{irs}^2, respectively. In the case that both paths exist, the channel gain can be found as:

$$\begin{aligned}|H(f)|^2 &= H(f)H^*(f)\\ &= G_{\mathrm{los}}^2 + G_{\mathrm{irs}}^2 + 2G_{\mathrm{los}}G_{\mathrm{irs}}\cos(2\pi f\Delta\tau), \end{aligned} \quad (9)$$

where $*$ is the complex conjugate and $\Delta\tau = \tau_{\mathrm{irs}} - \tau_{\mathrm{los}}$ is the relative delay between the LoS path and the IRS path. In an IRS assisted VLC system, the improvement brought by IRS compared to the case with LoS channel only is of

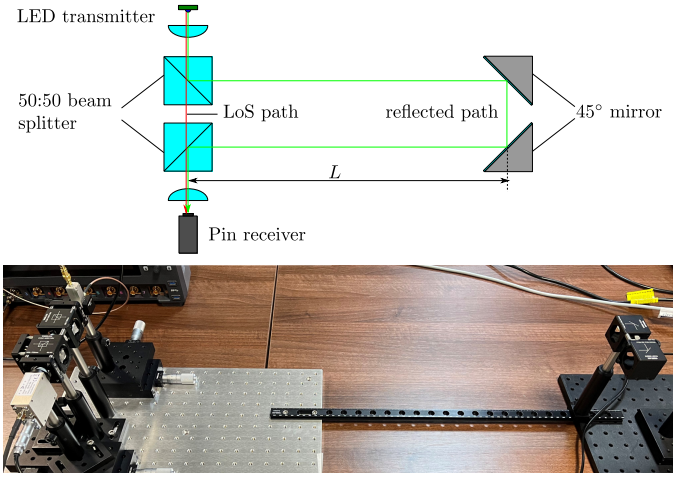

Figure 2: Experimental setup for single IRS element model validation.

concern. Therefore, we normalise the channel gain (9) by the LoS channel gain as:

$$\left|\tilde{H}(f)\right|^2 = \frac{|H(f)|^2}{G_{\text{los}}^2} = 1 + \tilde{G}^2 + 2\tilde{G}\cos(2\pi f \Delta\tau), \quad (10)$$

where $\tilde{G} = G_{\text{irs}}/G_{\text{los}}$ is the IRS to LoS channel path loss ratio. It can be observed that (10) is a simple periodic function of $\tilde{G}$ and $\Delta\tau$ in frequency domain, where $\tilde{G}$ determines the fluctuation and bias of the function and $\Delta\tau$ determines the period of the function. According to (10), $|\tilde{H}(f)|^2$ could be less than unity at some frequency, which means that the deployment of IRS is not always beneficial. The normalised channel gain is a convenient parameter for determining the improvement achieved by using IRS array as the performance of the LoS only scenario corresponds to the normalised channel gain at 0 dB. By solving the inequality $\frac{|H(f)|^2}{G_{\text{los}}^2} = 1 + \tilde{G}^2 + 2\tilde{G}\cos(2\pi f\Delta\tau) \geq 1$, it can be concluded that the IRS array improves the channel at frequencies in the range of $-\frac{1}{2\pi\Delta\tau}\arccos(-\frac{\tilde{G}}{2}) + \frac{l}{\Delta\tau} \leq f \leq \frac{1}{2\pi\Delta\tau}\arccos(-\frac{\tilde{G}}{2}) + \frac{l}{\Delta\tau}$ for any integer l and $\tilde{G} \leq 2$. Otherwise, the IRS array degrades the channel at other frequencies.

A. Experimental validation

To test whether the variance of channel gain against frequency is consistent with the single IRS element model described by (10), a proof-of-concept experiment was conducted. In particular, the impacts of relative delay $\Delta\tau$ and path loss ratio $\tilde{G}$ were validated. The experimental setup is shown in Fig. 2, which is designed to mimic the scenario with two propagation paths with different delays. A pair of LED transmitter and positive-intrinsic-negative (PIN) PD receiver together with aspherical lenses are deployed to form a short range LoS propagation path. Two 50:50 beam splitters are deployed along the LoS path. The first beam splitter allows approximately 50% of the light travel along the LoS path and the remaining light is reflected to the right hand side of the LoS path. At a distance of L away from the first beam splitter, we deploy two 45°mirrors which form a retro reflector and change the light propagation direction by 180°. The returning light can be collected by the second beam splitter. It combines the reflected light with the LoS light. Eventually, the combined light is detected by the PIN receiver. The reflected path is $2L$ longer than the LoS path, which leads to a relative propagation delay of $\Delta\tau = 2L/c$. Therefore, the relative propagation delay can be adjusted by changing the distance L. The lens at the receiver end is used to concentrate the incident light at the focal point of the lens. By placing the detector of the PIN PD receiver at the focal point, the received optical power via both the LoS and reflected paths is expected to be maximised. However, the implemented optical setup is not perfect, and the spatial points where the light concentrates via the LoS and reflected paths are not exactly collocated. Consequently, it is not possible to find an alignment to maximise the received optical power from both paths. Alternatively, the detector alignment is adjusted so that a reasonable amount of optical power from both paths is received. Interestingly, we can utilize this feature to manually control the proportion of power from the two propagation paths by slightly adjusting the alignment. Thus, the path loss ratio $\tilde{G}$ can be manipulated. Note that by using this power control mechanism, it is possible to achieve a wide range of path loss ratio. For example, the power from reflected path can be greater than that from the LoS path.

In this experiment, we measured the channel gain values in three different configurations of reflected path distances ($L = 30, 55, 80$ cm) and detector alignments. The estimation of the relative delays is straightforward by $\Delta\tau_{\text{mea}} = 2L/c = 2, 3.67, 5.33$ ns. In order to obtain the path loss ratio estimations and the measured normalised channel gains, three channel gain measurements with LoS path only, with a reflected path only and with both paths must be conducted in each configuration. The channel gain measurement results in the three configurations are shown in Fig. 3 (a), (b) and (c), respectively. All these results exhibit a low-pass characteristic due to the limited bandwidths of optical front-ends. In addition, the results of systems with both LoS and IRS paths show greater fluctuations with frequency, which are due to the channel characteristics of the free-space single IRS element model described by (8), (9) and (10). To understand the approach to estimate path loss ratio and the measured normalised channel gains, the measured channel gains with LoS path only, with a reflected path only and with both paths can be described by:

$$\left|H_{\text{mea}}^{\text{los}}(f)\right|^2 = |H_{\text{fe}}(f)|^2 G_{\text{los}}^2, \quad (11)$$

$$\left|H_{\text{mea}}^{\text{irs}}(f)\right|^2 = |H_{\text{fe}}(f)|^2 G_{\text{irs}}^2, \quad (12)$$

$$\left|H_{\text{mea}}^{\text{los+irs}}(f)\right|^2 = |H_{\text{fe}}(f)|^2 |H(f)|^2, \quad (13)$$

respectively, where $H_{\text{fe}}(f)$ represents the frequency response of the front-end channel. With (11) and (12), it is intuitive to estimate the path loss ratio by:

$$\sqrt{\frac{|H_{\text{mea}}^{\text{irs}}(f)|^2}{|H_{\text{mea}}^{\text{los}}(f)|^2}} = \sqrt{\frac{|H_{\text{fe}}(f)|^2 G_{\text{los}}^2}{|H_{\text{fe}}(f)|^2 G_{\text{irs}}^2}} = \frac{G_{\text{los}}}{G_{\text{irs}}} = \tilde{G}_{\text{mea}}. \quad (14)$$

Note that in this operation, the effects of font-end low path are cancelled out. The path loss ratio estimation results in the three

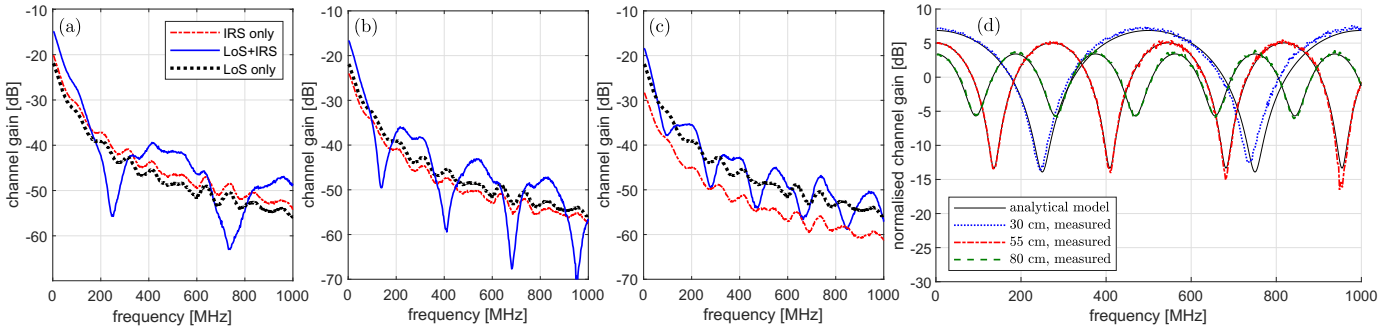

Figure 3: (a) Measured channel gains for $L = 30$ cm. (b) Measured channel gains for $L = 55$ cm. (c) Measured channel gains for $L = 80$ cm. (d) Normalised channel gain based on measurement and analytical model.

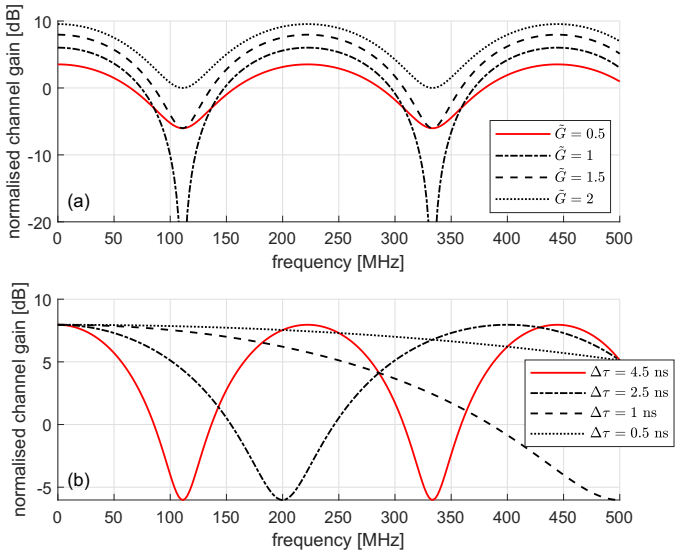

Figure 4: (a) Normalised channel gain against frequency with $\tilde{G} = 0.5, 1, 1.5, 2$ and $\Delta\tau = 4.5$ ns. (b) Normalised channel gain against frequency with $\Delta\tau = 4.5, 2.5, 1, 0.5$ ns and $\tilde{G} = 1.5$.

configurations are $\tilde{G}_{\text{mea}} = 1.244, 0.799, 0.5$, respectively. Next, the analytical results of normalised channel gain can be obtained by inserting the estimated parameters $\Delta\tau_{\text{mea}}$ and $\tilde{G}_{\text{mea}}$ into (10). Similar to the path loss ratio estimation, the measured normalised channel gain can be obtained by calculating the ratio of (13) to (11) as:

$$\frac{\left|H_{\text{mea}}^{\text{los+irs}}(f)\right|^2}{\left|H_{\text{mea}}^{\text{los}}(f)\right|^2} = \frac{|H_{\text{fe}}(f)|^2|H(f)|^2}{|H_{\text{fe}}(f)|^2 G_{\text{los}}^2} = \left|\tilde{H}_{\text{mea}}(f)\right|^2. \quad (15)$$

The analytical and measured normalised channel gain results in the three configurations are plotted in Fig. 3 (d). The close match between the analytical and measured results in all configurations validates the single IRS element model described by (8), (9) and (10). Despite the existence of low pass characteristics due to front-ends in practice, we intend to focus on investigating the characteristics caused by IRS-induced time delay in this work. Therefore, the low pass effects due to front-ends are not considered in the following sections.

B. Impacts of path loss ratio and relative time delay

By inspecting (10), it is apparent that the path loss ratio $\tilde{G}$ and the relative delay $\Delta\tau$ are key quantities, which determines the characteristics of the IRS-assisted VLC channel and the corresponding communication performance. The impact of varying $\tilde{G}$ and $\Delta\tau$ are investigated in this subsection. Expression (10) shows that the maximum and minimum value of the normalised channel gain is related to $\tilde{G}$ by $(1+\tilde{G})^2$ and $(1-\tilde{G})^2$, respectively. Fig. 4 (a) shows the normalised channel gain results against frequency with different $\tilde{G}$. With an increase of $\tilde{G}$ from 0.5 to 2, the maximum value of the normalised channel gain increases consistently from 3.52 dB to 9.54 dB. The minimum value of the normalised channel gain reaches zero when $\tilde{G} = 1$, which is similar to the deep fading in wideband RF wireless communications. The cases with $\tilde{G} = 0.5$ and 1.5 lead to an identical minimum normalised channel gain of -6.02 dB. When $\tilde{G} = 2$, a minimum value of the normalised channel gain increases to 0 dB, which implies that the IRS array improves the channel gain at all frequencies if $\tilde{G} > 2$. The period of the normalised channel gain in frequency domain is related to $\Delta\tau$ by $1/\Delta\tau$. The normalised channel gain reaches the minima at $f = \frac{l}{\Delta\tau} + \frac{1}{2\Delta\tau}$ and reaches the maximum at $f = \frac{l}{\Delta\tau}$ for any integer l, respectively. Fig. 4 (b) shows the normalised channel gain results against frequency with different $\Delta\tau$. It can be observed that when $\Delta\tau = 4.5$ ns, the normalised channel gain reaches the first minimum value at $f = 111$ MHz. When $\Delta\tau$ drops to 2.5 ns, the first minimum value of the normalised channel gain shift to $f = 200$ MHz. A communication system with a symbol period of T_{s} only uses a limited bandwidth of $1/2T_{\text{s}}$ and only channel gains within the modulation bandwidth matter to the performance. If the frequency of the first minimum normalised channel gain is within the modulation bandwidth ($1/2\Delta\tau < 1/2T_{\text{s}}$), the communication performance will be degraded. In time domain, this condition corresponds to $\Delta\tau/T_{\text{s}} > 1$. Therefore, the ratio of relative delay to the symbol period $\Delta\tau/T_{\text{s}}$ is a more crucial quantity than the exact value of $\Delta\tau$ and we define $\Delta\tau/T_{\text{s}}$ as a normalised delay.

Next, we evaluate the impact of $\tilde{G}$ and $\Delta\tau/T_{\text{s}}$ on the IRS-assisted VLC system performance with PAM-SCFDE by using (5) and (7). The simulated VLC system considers a 2.5 m LoS path channel with a perfect alignment. The remaining parameters are listed in Table I. This configuration leads to a LoS channel path loss of $G_{\text{los}} = 6.29 \times 10^{-6}$ with (1). Then, the channel gain in (5) can be obtained via (10) by $|H(f)|^2 = G_{\text{los}}^2 \left|\tilde{H}(f)\right|^2$ with $f = \frac{k}{KT_{\text{s}}}$ so that the impacts of

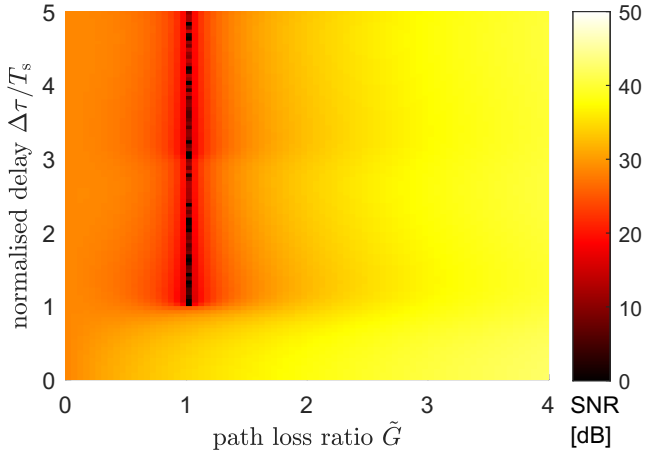

Figure 5: PAM-SCFDE received SNR against path loss ratio and normalised delay.

Table I

Parameters	Symbol	Values
LED optical power [W]	P_{opt}	2.5
LED half-power semiangle	$\phi_{1/2}$	60°
PD responsivity [A/W]	R_{pd}	0.6
PD detection area [cm^2]	A_{d}	1
PD FoV	ψ_{fov}	90°
Symbol period [ns]	T_{s}	1
FFT size	K	512
PAM modulation order	M	16
Absolute temperature [K]	$\mathcal{T}_{\text{a}}$	300
Receiver load resistance [Ω]	R_{L}	50
IRS reflectivity	ρ	1
CP length	L_{cp}	50
Modulation scaling factor	κ	3.2
Gap value	Γ	1
IRS array size (Section V)	$N_{\text{x}} \times N_{\text{y}}$	5×3

$\tilde{G}$ and $\Delta\tau$ can be incorporated. The received SNR numerical results are shown in Fig. 5. The BER numerical results against channel path loss ratio and those against relative delay are shown in Fig. 6 and Fig. 7, respectively. Note that both $\tilde{G}$ and $\Delta\tau/T_{\text{s}}$ are ratios and dimensionless. Fig. 6 and Fig. 7 show the BER results generated by link level simulations with red makers, which matches the analytical results (7) well. In addition, (7) is a BER lower bound, which only considers the errors between adjacent symbols and underestimates the value in the high BER region, ie., BER greater than 1×10^{-1}. It can be observed that when $\tilde{G} = 1$, the achievable SNR is extremely low and the corresponding BER is greater than 1×10^{-1}. Note that this performance degradation is not due to the missing of channel equalisation module. In the considered PAM-SCFDE system, a ZF equalisation is used. However, there are channel gain nulls at some frequencies due to the destructive combination of signals via the LoS and the IRS paths, as shown in Fig. 4 (a). The resultant SNR of PAM is determined by channel gains across the entire modulation bandwidth. Therefore, the equalisation is unable to effectively mitigate the severe channel distortion and leads to a low SNR. The exception cases are those with narrowband systems ($\Delta\tau/T_{\text{s}} < 1$), where the lowest frequency that leads to zero normal channel gain exceeds the modulation bandwidth.

In Fig. 5, it can be observed that the SNR is high when $\tilde{G}$

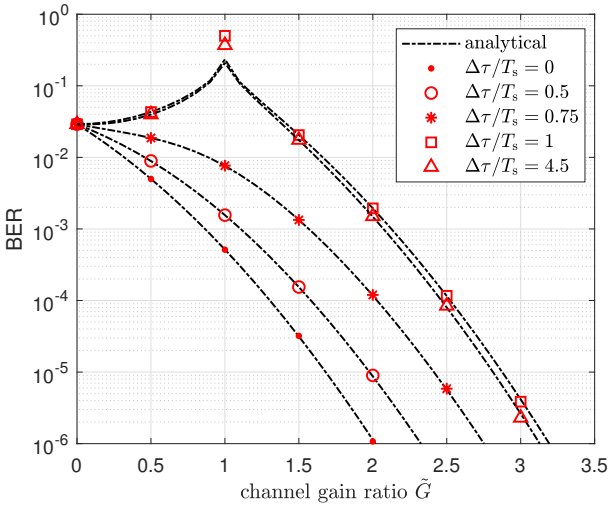

Figure 6: BER against path loss ratio.

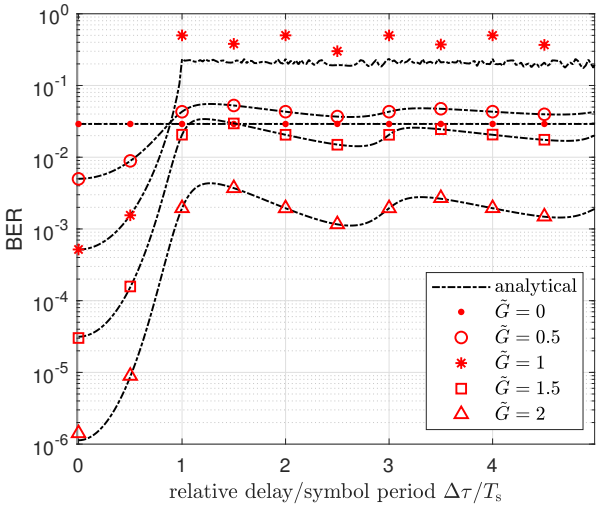

Figure 7: BER against relative delay spread.

is greater than 2. This is because the light via IRS improves significantly and starts to dominate the channel. The SNR is also greater when $\Delta\tau/T_{\text{s}}$ is less than one. This is because most of the signal power via the LoS path and IRS paths fall in the same symbol slot, which leads to a narrowband system with minor inter-symbol interference (ISI) issue. Fig. 6 shows that the BER decreases with an increase of $\tilde{G}$ when $\Delta\tau/T_{\text{s}} < 1$. In the case with $\Delta\tau/T_{\text{s}} > 1$, the BER first increases with $\tilde{G}$ and reaches the peak at $\tilde{G} = 1$. Then, the BER start to decrease with $\tilde{G}$. Considering the impact of the normalised delay, when $\Delta\tau/T_{\text{s}}$ is much less than unity, the combinations of the IRS and the LoS channels are mostly constructive and lead to an improved performance. Fig. 7 shows that a lower BER can be achieved compared to the case with $\tilde{G} = 0$ when $\Delta\tau/T_{\text{s}}$ is close to zero. When $\Delta\tau/T_{\text{s}}$ getting closer to unity, the system starts to be in wideband and its modulation bandwidth starts to cover the frequency of the first minimum normalised channel gain. Consequently, the SNR drops quickly and the BER increases severely, as shown in

Fig. 5 and Fig. 7. When $\Delta\tau/T_{\rm s}$ increases further, the BER start to fluctuate around a certain level as there are both constructive and destructive combinations. In summary, the IRS array consistently improves the communication performance of a narrowband VLC systems with $\Delta\tau/T_{\rm s} < 1$. However, in the cases of wideband VLC systems with $\Delta\tau/T_{\rm s} \geq 1$, the communication performance is likely to degrade when LoS and IRS components are comparable ($\tilde{G} \approx 1$). This degradation occurs because the IRS-induced delay leads to frequency selectivity and severe destructive combinations at certain frequencies. When the channel is dominated by IRS components ($\tilde{G} \geq 2$), IRS array provides a consistent communication performance improvement to VLC systems.

IV. Achievable rate analysis of IRS-assisted VLC

Section III demonstrated the performance degradation due to the IRS-induced time delay with a PAM-SCFDE modulation, where SNR is determined by the channel response over the entire modulation bandwidth. A straightforward solution to alleviate this degradation is to use multi-carrier modulation (MCM) schemes, such as OFDM. Thus, the frequency selective channel can be divided into a number of flat sub-channels. The modulation order on different sub-channel can be adjusted adaptively so that excessive BER can be avoided. Therefore, an achievable rate analysis of IRS-assisted VLC systems with DCO-OFDM is presented in this section to evaluate the impacts of IRS-induced time delay on the communication performance. The achievable rate of a DCO-OFDM system with a frequency-selective channel can be calculated as [22], [23]:

$$R = \int_0^{\frac{1}{2T_{\rm s}}} \log_2\left(1 + \frac{2T_{\rm s}E(f)P_{\rm opt}^2|H(f)|^2R_{\rm pd}^2}{\Gamma\kappa^2N_0}\right)\mathrm{d}f, \quad (16)$$

where κ is the modulation scaling factor for DCO-OFDM and $E(f)$ is a power allocation factor and Γ is a gap value to compensate for the imperfection of practical modulation and coding.

A. Power allocation schemes

The configuration of the power allocation factor must fulfil a total transmission power constraint:

$$2T_{\rm s}\int_0^{\frac{1}{2T_{\rm s}}} E(f)\mathrm{d}f = 1. \quad (17)$$

Two power control policies are considered in this paper. The first one uses a uniform power allocation, which distributes the transmission power evenly $E(f) = 1$ in the frequency range of $1/2T_{\rm s}$. This power allocation strategy has low computation complexity. The second power control strategy uses a waterfilling optimisation approach, which can maximise the achievable rate under the total transmission power constraint (17). The corresponding optimal power allocation factor can be found as [22]:

$$E\left(f\right) = \left(\frac{1}{\lambda} - \frac{\Gamma\kappa^2N_0}{2T_{\rm s}P_{\rm opt}^2\left|H\left(f\right)\right|^2R_{\rm pd}^2}\right)^+, \quad (18)$$

where $\frac{1}{\lambda}$ is the 'water level' constant, which can be obtained by a bisection search method. The operator $(\cdot)^+$ is defined as:

$$u^+ = \begin{cases} u & \text{if } u > 0 \\ 0 & \text{if } u \leq 0 \end{cases}. \quad (19)$$

As shown in (18), the value of power allocation factor depends on the channel gain $|H\left(f\right)|^2$, which requires channel information and higher computational complexity.

By inserting (4) into (16) with $\mathbf{1}_{\rm los} = \mathbf{1}_{\rm irs} = 1$, the achievable rate with an IRS array can be calculated by:

$$R = \int_0^{\frac{1}{2T_{\rm s}}} \log_2\left(1 + \frac{2T_{\rm s}E(f)P_{\rm opt}^2R_{\rm pd}^2}{\Gamma\kappa^2N_0} \times \left|G_{\rm los}\mathrm{e}^{-2\pi jf\tau_{\rm los}} + \sum_{i=1}^{N_{\rm irs}} G_i\mathrm{e}^{-2\pi jf\tau_i}\right|^2\right)\mathrm{d}f. \quad (20)$$

B. Closed-form solution with a single IRS element model and uniform power allocation

In the case of uniform power allocation $E(f) = 1$, the channel gain only exists in the numerator inside the log term. In the case of single IRS element, the achievable rate (20) can be simplified as:

$$R = \int_0^{\frac{1}{2T_{\rm s}}} \log_2\left(1 + \frac{2T_{\rm s}P_{\rm opt}^2R_{\rm pd}^2}{\Gamma\kappa^2N_0}\left|G_{\rm los}\mathrm{e}^{-2\pi jf\tau_{\rm los}} + G_{\rm irs}\mathrm{e}^{-2\pi jf\tau_{\rm irs}}\right|^2\right)\mathrm{d}f = \int_0^{\frac{1}{2T_{\rm s}}} \log_2\left(1 + \Lambda \times \left(G_{\rm los}^2 + G_{\rm irs}^2 + 2G_{\rm los}G_{\rm irs}\cos 2\pi f\Delta\tau\right)\right)\mathrm{d}f, \quad (21)$$

where $\Lambda = \frac{2T_{\rm s}P_{\rm opt}^2R_{\rm pd}^2}{\Gamma\kappa^2N_0}$ is a constant factor irrelevant to frequency f. With further rearrangement and derivation, a closed-form solution to (21) can be concluded as (22). Note that the derivation of the integral $\int_0^B \log_2\left(1 + A\cos(2\pi f\Delta\tau)\right)\mathrm{d}f$ with $A = \frac{2G_{\rm los}G_{\rm irs}}{\Lambda^{-1}+\left(G_{\rm los}^2+G_{\rm irs}^2\right)}$ and $B = \frac{1}{2T_{\rm s}}$ in step (a) of (22) is presented in the Appendix A. In addition, the series in (22) is convergent, which is proved in Appendix B. Therefore, (22) can be evaluated by calculating the first $l_{\max}$ terms.

In Fig. 8, the result of (22) is plotted against the path loss ratio and normalised delay, which is similar to Fig. 5 except for the change of metric from PAM SNR to DCO-OFDM achievable rate. The system parameter configurations are identical to those listed in Table I. In general, the achievable rate performance exhibits a similar trend to that in terms of PAM SNR. When the normalised delay is smaller than one, the system is behaving as a narrowband communication system. Consequently, increasing the path loss ratio will consistently improve the system achievable rate. With a path loss ratio of zero, the achievable rate is 2.86 Gbps. By increasing the path loss ratio to two, the achievable rate can reach a level above 4 Gbps. In the case of wideband communication system with a normalised delay greater than one, very limited improvement in achievable rate ($<$ 3 Gbps) is observed if the path loss ratio is less than one. With some normalised delay values (e.g. 1-2 and 3-4), the achievable rates are slightly less than those without IRS (2.6-2.7 Gbps). Nevertheless, the

$$
\begin{aligned}
R &= \frac{1}{2T_{\mathrm{s}}}\log_2\left(1+\Lambda\left(G_{\mathrm{los}}^2+G_{\mathrm{irs}}^2\right)\right)+\int_0^{\frac{1}{2T_{\mathrm{s}}}}\log_2\left(1+\frac{2G_{\mathrm{los}}G_{\mathrm{irs}}\cos(2\pi f\Delta\tau)}{\Lambda^{-1}+\left(G_{\mathrm{los}}^2+G_{\mathrm{irs}}^2\right)}\right)\mathrm{d}f \\
&\overset{(a)}{=} \frac{1}{2T_{\mathrm{s}}}\log_2\left(1+\Lambda\left(G_{\mathrm{los}}^2+G_{\mathrm{irs}}^2\right)\right)+\frac{1}{2\pi\Delta\tau\ln 2}\sum_{l_1=1}^{\infty}\frac{(-1)^{2l_1}}{(2l_1-1)2^{2(l_1-1)}}\left(\frac{2G_{\mathrm{los}}G_{\mathrm{irs}}}{\Lambda^{-1}+\left(G_{\mathrm{los}}^2+G_{\mathrm{irs}}^2\right)}\right)^{2l_1-1} \\
&\times\left(\sum_{l_2=0}^{l_1-1}\binom{2l_1-1}{l_2}\frac{\sin\left(\frac{2\pi\Delta\tau}{2T_{\mathrm{s}}}(2l_1-2l_2-1)\right)}{2l_1-2l_2-1}\right)+\frac{(-1)^{2l_1+1}}{2l_1 2^{2l_1}}\left(\frac{2G_{\mathrm{los}}G_{\mathrm{irs}}}{\Lambda^{-1}+\left(G_{\mathrm{los}}^2+G_{\mathrm{irs}}^2\right)}\right)^{2l_1} \\
&\times\left(\frac{\pi\Delta\tau}{T_{\mathrm{s}}}\binom{2l_1}{l_1}+2\sum_{l_2=0}^{l_1-1}\binom{2l_1}{l_2}\frac{\sin\left(\frac{2\pi\Delta\tau}{2T_{\mathrm{s}}}(2l_1-2l_2)\right)}{2l_1-2l_2}\right)
\end{aligned}
\tag{22}
$$

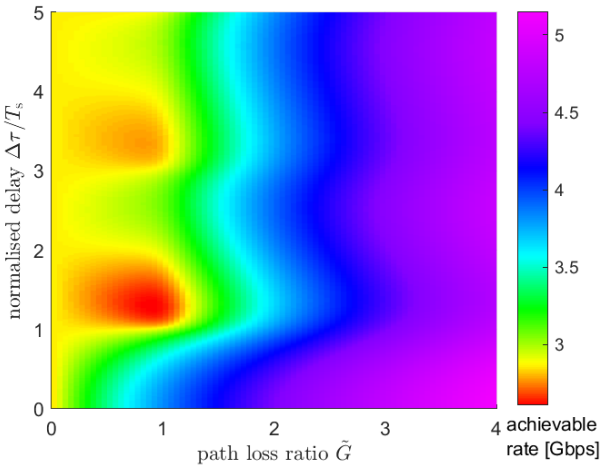

Figure 8: DCO-OFDM achievable rate against path loss ratio and normalised delay.

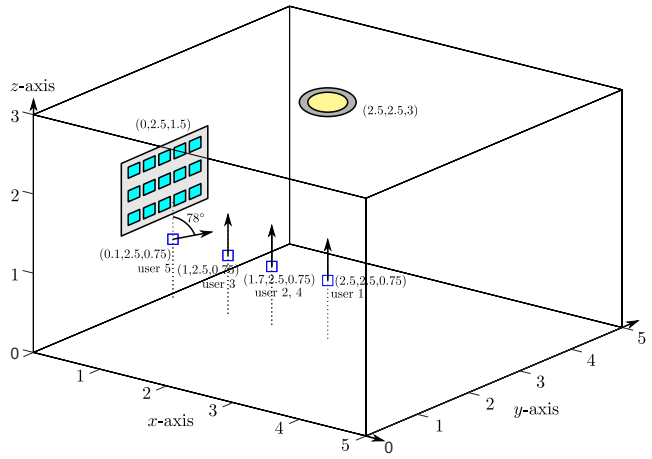

Figure 9: Geometry of the considered indoor environment.

achievable rate performance in this regime is much better than the SNR performance with PAM-SCFDE. This is because the performance of single-carrier modulation, like PAM, depends on the channel quality across the whole modulation bandwidth. When the path loss ratio is much greater than one (IRS reflected signal is stronger than that via the LoS path), the achievable rate increases consistently.

V. Simulation results in a practical scenario

In practice, the values of $\tilde{G}$ and $\Delta\tau$ are subject to the user position and orientation. Therefore, it is important to evaluate the impact of IRS time delay on the performance of a VLC system with a practical setup. In the following simulations, the considered indoor environment has a dimension of $5\ \mathrm{m}\times 5\ \mathrm{m}\times 3\ \mathrm{m}$, as shown in Fig. 9. An LED transmitter is deployed in the centre of the room at the ceiling level $(2.5, 2.5, 3)$ with an orientation towards the floor $(0, 0, -1)$. The PD receivers are positioned at the desktop level with a straight upward orientation $(0, 0, 1)$. The remaining system parameters are the same as those listed in Table I if they are not specified.

A. Effects of multi-element IRS array and inter-element separation

In reality, a single IRS element is unlikely to provide a high gain, such as $\tilde{G} > 1$. Therefore, an IRS array with multiple reflecting elements are necessary to improve the gain. However, each IRS element has a slightly different position relative to other IRS elements, and the propagation delays of reflection paths via different elements vary. This may lead to a different channel behaviour compared to the single IRS element model. Therefore, we evaluate the normalised channel gains with various separation between adjacent IRS elements D_{a} (see Fig. 1) so that the effects of these multiple delays can be quantified. We assume that a 5×3 IRS array is deployed on the centre of a wall $(0, 2.5, 1.5)$ with an orientation of $(1, 0, 0)$ and a user is located at $(1, 2.5, 0.75)$. The normalised channel gains against frequency with different values of D_{a} are shown in Fig. 10. When $D_{\mathrm{a}} = 0$ cm, the normalised channel gains are the highest. However, this is not practical as all IRS elements are collocated, but the performance of this setup is identical to the case with a single IRS element, which can be used as a reference. When $D_{\mathrm{a}} = 10$ cm, the normalised channel gains are slightly lower and the channel function period is also slightly shorter. This is because the average propagation distance via each element is slightly longer, so that the path loss via IRS becomes more severe and the propagation

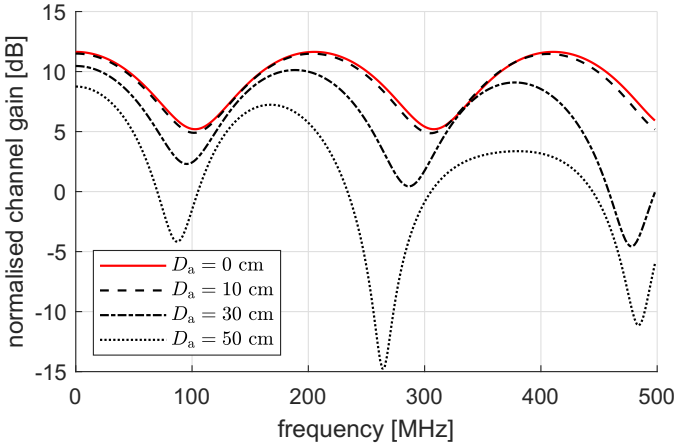

Figure 10: Normalised channel gains against frequency with different separation between adjacent IRS elements D_a.

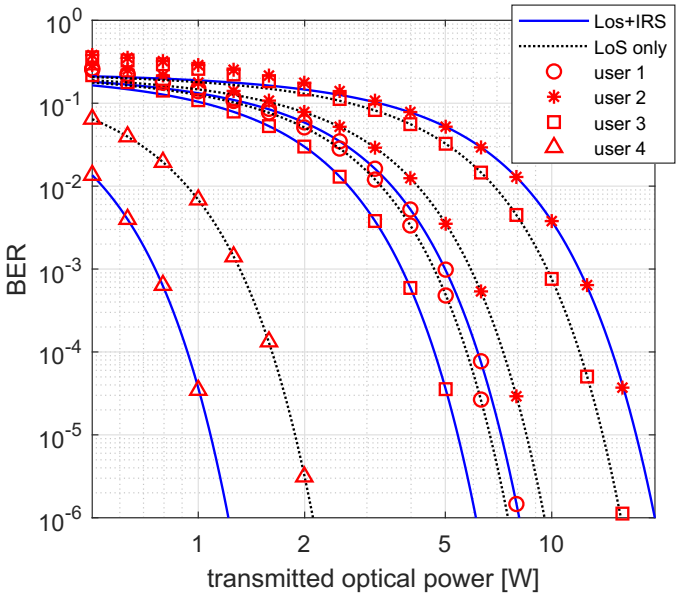

Figure 11: Results of BER against optical power of different users. User 1 is located at $(2.5, 2.5, 0.75)$, user 2 is located at $(1.7, 2.5, 0.75)$, user 3 is located at $(1, 2.5, 0.75)$ and user 4 is collocated with user 2 but the symbol period is changed to $\Delta\tau/T_s = 20$ ns.

Table II: Results of path loss ratio and normalised delay

	user 1	user 2	user 3	user 4	user 5
$\tilde{G}$	0.36	0.86	2.76	0.86	0.766
$\Delta\tau/T_s$	10.95	7.99	4.92	0.4	1.33

delay is longer. Nevertheless, the single element model can still accurately characterise the channel with $D_a = 10$ cm. When D_a increases further to 30 cm and 50 cm, the channel degradation and the shortening of the channel function period becomes more severe. In addition, the channel start to exhibit a low pass characteristic, which is due to the fact that the CIR (caused by the multiple IRS elements) spanned in a wider time range (increased delay spread of the reflected components). The issue of statistical independence between multiple closely deployed IRS elements in RF wireless systems is negligible in IM/DD-based VLC system, where the effects of small-scale fading can be omitted [11]. Furthermore, the considered IRS separations in the order of centimetres are significantly greater than the wavelength in the visible light range. These results demonstrate that the proposed single-element model can capture the characteristics of the IRS-assisted VLC channel when D_a is small. In addition, it can be observed that a VLC system with a clustered IRS array (small D_a) outperforms that with a distributed IRS array (large D_a).

B. BER performance of different users

Based on the results in Section V-A, the scenario with $D_a = 10$ cm is used in the following results as it leads to the desired performance and is also practical for implementation. Next, we evaluate the communication performance of four users at different positions or with different settings. The positions of the four users are illustrated in Fig. 9. The BER results are shown in Fig. 11. The close match between the link level simulation results (red markers) and the analytical results (curves) validates the evaluation. To validate the findings presented in Section III-B, we also evaluate the path loss ratio $\tilde{G}$ and the normalised delay $\Delta\tau/T_s$. However, due to the use of multi-element IRS array, there are multiple IRS path losses G_i and IRS delays τ_i corresponds to the ith IRS element. Therefore, we decide to modify the path loss ratio and relative delay as $\tilde{G} = \sum_{i=1}^{N_{irs}} G_i/G_{los}$ and $\Delta\tau = \sum_{i=1}^{N_{irs}} (\tau_i - \tau_{los})/N_{irs}$, respectively. The results of $\tilde{G}$ and $\Delta\tau/T_s$ are listed in Table II.

As shown in Fig. 9, the first user is in the centre of the room underneath the LED $(2.5, 2.5, 0.75)$, which leads to a relatively strong LoS path and weak IRS paths. Consequently, the resultant $\tilde{G}$ is only 0.36, as shown in Table II. In addition, the reflected paths are much longer than the LoS path. This leads to a normalised delay of 10.95 which is much higher than one. Fig. 11 shows that the BER with assistance of IRS array is slightly higher than the case with the LoS channel only. The required optical power to reach a BER of 1×10^{-3} with an IRS array is 7% higher than the case with LoS path only. These observations are consistent with the analysis in Section III-B. User 2 is located at $(1.7, 2.5, 0.75)$, which is closer to the IRS array compared to user 1. The resultant path loss ratio is 0.86, which is very close to unity and leads to severe multipath destructive combinations. Fig. 11 shows that the BER achieved by IRS assisted system is severely degraded compared to the case with the LoS channel only. The required optical power to reach a BER of 1×10^{-3} with an IRS array is over 100% more than the case with LoS path only. The results of user 1 and user 2 demonstrate that the IRS-induced time delay could lead to worse communication performance by using an IRS array in practice, and the IRS array should be deactivated for these users. User 3 is next to the IRS array $(1, 2.5, 0.75)$, which leads to a strong IRS channel. The resultant $\tilde{G}$ and $\Delta\tau/T_s$ are 2.76 and 4.92, respectively. Fig. 11 shows that the BER achieved by the IRS assisted system is significantly lower than that of the case with LoS channel only. The required optical power to reach a BER of 1×10^{-3} with an IRS array is reduced by 61.1% of that required in the case with LoS path only. This result demonstrates the promising benefits of deploying IRS arrays for users close to room edges in a VLC system. User 4 is collocated with user 2 except that the symbol

period increased to 20 ns. Due to the narrower bandwidth, the receiver noise variance is decreased with the same noise PSD. Consequently, the BER results are much lower than those of user 1 to 3. Despite that the resultant $\tilde{G}$ of 0.86 is close to one, but the VLC system uses a much smaller modulation bandwidth. Consequently, the value of $\Delta\tau/T_{\rm s}$ is only 0.4. As expected, the IRS array can still improve the BER performance in this case, as shown in Fig. 11. The required optical power to reach a BER of 1×10^{-3} with an IRS array is reduced by 42.4% compared to the case with LoS path only. The result of user 4 shows that the VLC systems using a narrower modulation bandwidth are less affected by the negative effects of IRS-induced time delay.

C. Achievable rate performance of different users

In Fig. 12, the achievable rate performance of user 1, 3 and 5 against optical power are demonstrated. In each subplot, four curves are plotted. The black solid curve is generated via analytical expression (22). Note that since the analytical expression considers a single IRS element, the variables $G_{\rm irs}$ and $\Delta\tau$ are filled with $G_{\rm irs} = \sum_{i=1}^{N_{\rm irs}} G_i$ and $\Delta\tau = \sum_{i=1}^{N_{\rm irs}} (\tau_i - \tau_{\rm los})/N_{\rm irs}$, respectively. The red curves with circular and asterisk markers are numerical evaluations of achievable rates (20) with uniform and waterfilling power allocations, respectively. The blue curves with triangle markers shows the achievable rate of the VLC systems without IRS, which can be evaluated by (16) with $H(f) = G_{\rm los}$. Note that the analytical results of (22) match closely with the numerical evaluations of (20) with the uniform power allocation for all users. This agreement not only validates the accuracy of the analytical expression, but also demonstrate that the proposed single-element IRS model can accurately reflect the performance of multi-element IRS-assisted VLC systems as long as the inter-element separation $D_{\rm a}$ is small.

In the case of user 1, the relative delay is over 10, as shown in Table II, which indicates a wideband VLC system. In addition, the path loss ratio is only 0.36. The achievable rates of the VLC systems with and without IRS array are almost the same, as shown in Fig. 12 (a), which agrees with the observation in Fig. 8. In the case of user 3, the user position is closer to the IRS array, as shown in Fig. 9, which leads to a greater path loss ratio of 2.76, as shown in Table II. Therefore, the achievable rate improvement by using IRS array is significant, as shown in Fig. 12 (b). At the same optical power level, the IRS array increases the achievable rate by about 1 Gbps. In the case of user 5, the user is next to the IRS array, but the detector has a 78° tilting angle, as shown in Fig. 9, which leads to a significant misalignment with both the LED transmitter and the IRS array. Consequently, the receiver optical power level is much lower than the other users. Therefore, the achievable rates are also the lowest. In addition, the path loss ratio and the relative delay for user 5 are 0.766 and 1.33, respectively, as shown in Table II. This falls in the regime where the IRS may lead to a slight achievable rate drop according to the observation in Fig. 8. As expected, the achievable rates of the VLC system without IRS array are slightly higher than those with the IRS array when the optical power is greater than 2 W, as shown in Fig. 12 (c). It is worth noting that the systems with uniform power allocation and waterfilling power allocation achieve almost the same data rate in most cases. The waterfilling power allocation outperforms the uniform power allocation obviously only for user 5 with low received optical power. This observation align with the conclusion in [22] that waterfilling is mostly useful when the communication system is power limited.

D. Random user performance

It is observed in Fig. 11 that the IRS array improves the performance of some users while degrading the performance of the others. Therefore, it is meaningful to investigate the statistical performance of a random user. Now, we consider the same indoor environment and system configuration shown in Fig. 9 and Table I with $D_{\rm a} = 10$ cm except for the user position. Here, we consider users positioned on a square grid so that the performance of users at various locations can be evaluated and compared. The spatial distribution of the path loss ratio and relative delay are plotted in Fig. 13 and Fig. 14, respectively. The IRS array is located at $(0, 2.5, 1.5)$, which corresponds to the bottom of the Fig. 13 and Fig. 14. It can be observed that those users close to the IRS array can achieve path loss ratio of between 5 to 15, while the users on the other end of the room achieve a path loss ratio close to zero. Fig. 14 shows that the relative delay is shorter for those users closer to the IRS array. However, most of the users achieve a relative delay greater than one with a symbol period of $T_{\rm s} = 1$ ns. The resultant SNRs with and without the assistance of IRS array are shown in Fig. 15 and Fig. 16, respectively. In cases without assistance of the IRS array, only users in the room centre can achieve a SNRs above 25 dB and the maximum SNR is below 30 dB. In cases with assistance of the IRS array, the SNRs of the users close to the IRS array are significantly improved up to 37 dB. However, the SNRs of some users in the region where x is between 1.5 and 2.5 are severely degraded to be less than 15 dB. This is because, the path loss ratio achieved by these users are close to one, as shown in Fig. 13.

Next, users with random positions and two orientation scenarios are considered. The first orientation scenario defines a straight upward user orientation, which is similar to those shown in Fig. 9. The second orientation scenario defines a random user orientation based on the work conducted in [24], where the orientation of each user is defined by a pan angle and a tilt angle. The pan angle follows a uniform distribution while the tilt angle follows a Laplace distribution with a mean of 41.39°and a standard deviation of 7.68°for seating users [24]. In addition, the cases with three IRS array positions are evaluated. The first IRS array position is at the centre of the wall $(0, 2.5, 1.5)$. The second position is moved to the left of the wall centre at $(0, 1.25, 1.5)$. The last position is moved up by 0.5 m compared to the wall centre position at $(0, 2.5, 2)$. The empirical CDF results of path loss ratio and relative delay are presented in Fig. 17 and Fig. 18, respectively. The empirical CDF is generated by collecting data from a large number of users with random positions/orientations. The collected data is sorted in ascending order, and the empirical

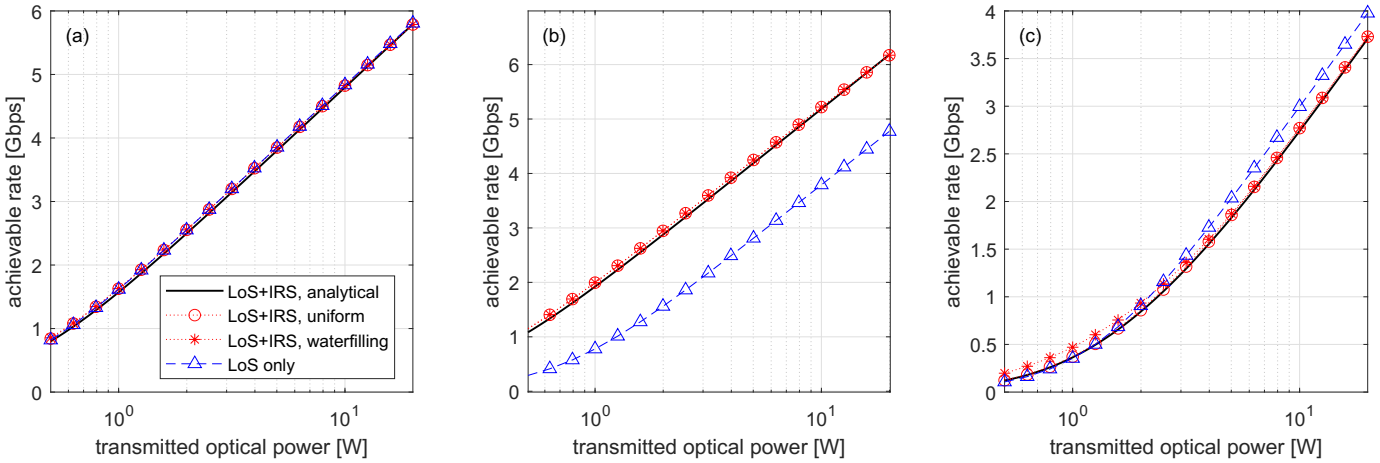

Figure 12: DCO-OFDM achievable rate against optical power. (a) user 1 (b) user 3 (c) user 5

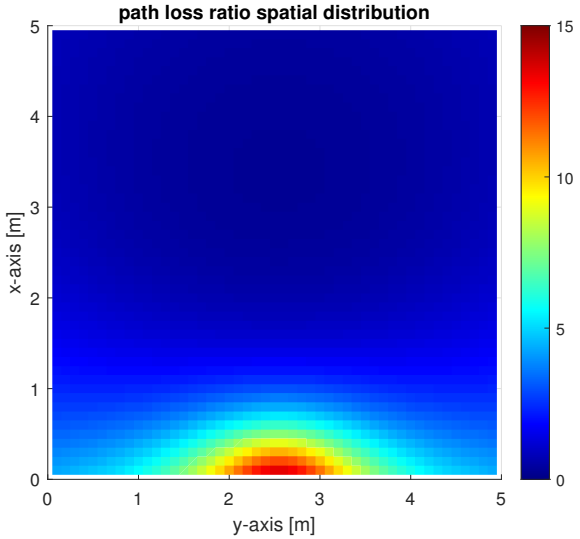

Figure 13: Path loss ratio of users at various positions.

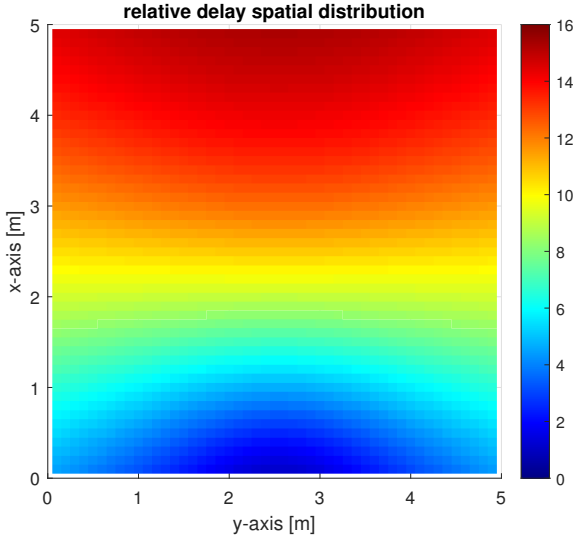

Figure 14: Relative delay of users at various positions.

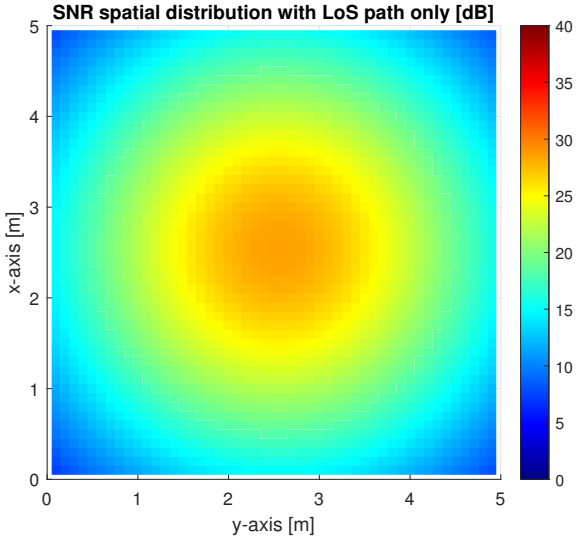

Figure 15: SNR of users at various positions with the LoS path only.

CDF is obtained by calculating the proportion of data points that are less than or equal to a specific threshold of interest. Regarding the statistics of path loss ratio, 70% to 85% of the users achieve path loss ratios of less than 2. About 21.8% to 48.8% of the users achieve path loss ratios of between 0.5 to 1.5. For users with random orientation, about 30% users receive zero reflected signals, because the IRS array is out of the receiver coverage with some random orientations. However, there is also a high probability that a user receiver with a random orientation is directed towards the IRS array, which leads to superior path loss ratio statistics in the range above one. Regarding the statistics of relative delay, all users achieve a relative delay above one and the highest relative delay could reach 15 to 17. Note that this result is subject to the communication symbol period T_s and the relative delay statistics for upward and random orientation scenarios are identical, because the time delay is irrelevant to receiver orientation.

The SNR statistics of users with upward and random orientation scenarios are shown in Fig. 19 and Fig. 20,

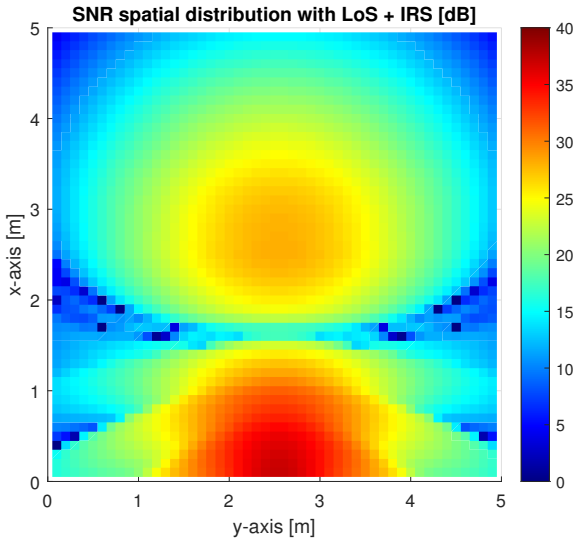

Figure 16: SNR of users at various positions with both LoS and the reflected paths by the IRS array.

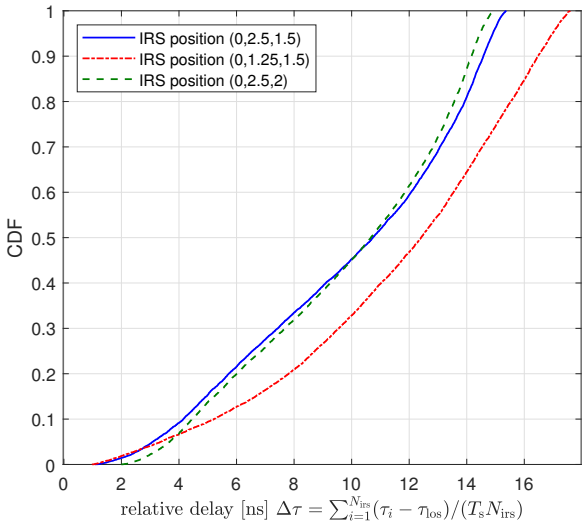

Figure 18: Relative delay CDF of users with random positions and orientations.

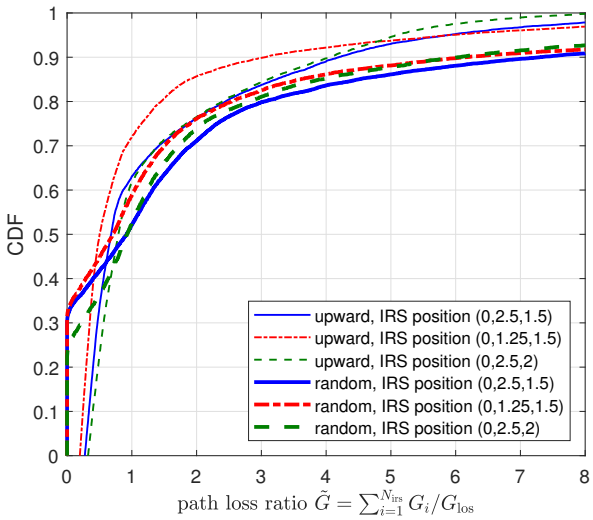

Figure 17: Path loss ratio cumulative distribution function (CDF) of users with random positions and orientations.

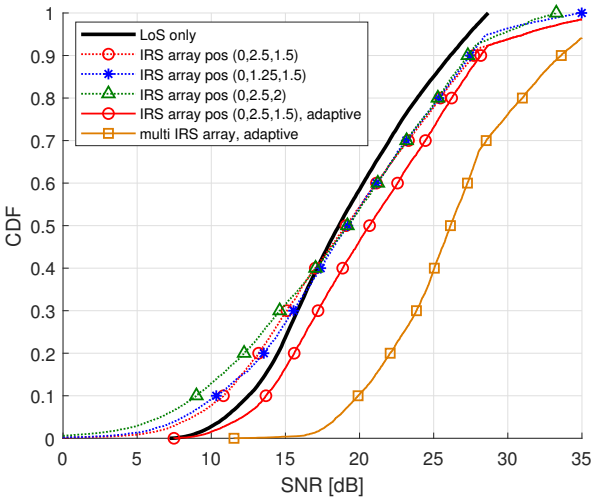

Figure 19: SNR CDF of users with random positions and the upward orientation.

respectively. In cases of upward orientation scenario, the IRS array improves the SNR statistics in the high SNR region ($\gamma > 20$ dB) compared to the case with the LoS path only, as shown in Fig. 19. This is because of the additional received optical power via reflection paths. However, the IRS array degrades the SNR statistics in the low SNR region ($\gamma < 15$ dB) due to the severe destructive combination with path loss ratio close to one. In cases with random orientation scenario, the communication performance of users based on the LoS path gets worse compared to cases with upward orientation scenario due to the higher probability of misalignment. Consequently, the use of IRS array could slightly compensate for this misalignment issue. Therefore, the IRS array improves the SNR statistics with all IRS array positions compared to the cases with the LoS path only. Note that about 10% of users achieved SNRs lower than 0 dB due to the undesired receiver orientation. Comparing the user performance with different IRS positions, the system with the IRS array located at $(0, 2.5, 1.5)$ achieves the best SNR statistics among the three considered IRS positions. A simple approach to avoid the SNR penalty is to adaptively active the IRS array, which turning on the IRS array only when it improves the SNR and disable the IRS otherwise. The results with the 'adaptive' approach for the IRS array located at $(0, 2.5, 1.5)$ are also included in Fig. 19 and Fig. 20, which shows superior performance compared to the results of other scenarios. Another approach to further enhance the user performance is to deploy multiple IRS arrays on each wall. In conjunction with the adaptive approach, the system could decide which IRS array to activate so that the achievable SNR can be maximised. The corresponding results are also shown in Fig. 19 and Fig. 20. It can be observed that the systems with multiple IRS arrays outperform systems with only one IRS array by approximately 5 to 10 dB in

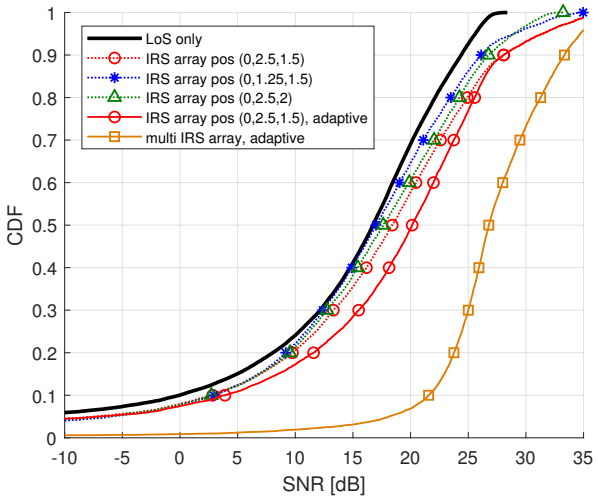

Figure 20: SNR CDF of users with random positions and random orientation.

terms of median SNR for both user orientation scenarios. For the random user orientation case, about 10% of users in systems with one IRS array experience SNRs below 0 dB. In the system with multiple IRS array, this number is reduced to about 1%. These results demonstrate that by deploying more IRS arrays and activate only the best array to assist the VLC system can dramatically improve the communication performance and mitigate the negative effects caused by IRS-induced time delay.

VI. Future Research Directions considering IRS-induced Time Delay Effects

The presented results in Section V show that there is a very high probability that activating the IRS array may degrade the VLC performance. In this undesired situation, deactivating the IRS array or switching some of the IRS elements off would lead to a more desired performance rather than activating the entire IRS array. Therefore, the consideration of the frequency domain channel characteristics of IRS-assisted VLC systems with time delay opens the door for many research directions to alleviate this negative effect caused by IRS-induced time delay or to utilize these special features to achieve specific targets, such as optimization of resource allocation and enhancement of physical layer security in VLC systems. In the following, we try to shed the light on some related research directions.

A. Channel Modelling with IRS-induced Time Delay and Mitigation of Its Effects

Most of the published research papers in the area neglect this IRS-induced time delay effect and assume that the LoS and reflected paths are constructively added at the receiver, which leads to enhancement in the perceived channel gain and, consequently, higher SNR and higher data rates. However, the results shown in this paper make it evident that such an assumption is too simplistic and does not reflect real-life scenarios. We believe that the future channel modeling of IRS-assisted VLC systems could take the IRS-induced time-delay into account. In addition, a potential solution to mitigate the effects of IRS-induced time delay can be explored. For example, the number of active IRS elements can be adjusted so that the path loss ratio could be controlled to avoid severe destructive combinations. Furthermore, OFDM could be used so that subcarriers with lower SNR could be unloaded and performance penalty can be avoided.

B. Optimization of Resource Allocation with IRS-induced Time Delay

Considering an IRS-assisted VLC system with a multi-user scenario, different users may have various channel frequency responses, which may introduce multi-user diversity. Transmission resources, such as time, frequency or IRS element, are allocated among users. Advanced optimisation tools could be used to find the best resource allocation solution so that the target performance metrics, such as aggregated data rate, can be maximized.

C. Physical Layer Security with IRS-induced Time Delay

The destructive effect of IRS-induced ISI can be utilised to enhance the physical layer security (PLS) in IRS-assisted VLC systems. More specifically, artificial jamming can be employed by activating the IRS elements that result in the lowest SNR at the eavesdropper, making it difficult for it to retrieve the confidential signal. Based on that, the secrecy capacity can be dramatically enhanced.

VII. Conclusion

In this paper, we have investigated the impact of IRS-induced time delay on the performance of an IRS-assisted VLC system. A proof-of-concept experiment has been conducted to demonstrate the considered issue. The research findings show that the use of IRSs can improve the received signal power dramatically in many cases, thereby enhancing the system SNR or achievable rate. However, care must be taken when deploying IRSs, as the delay between the LoS and the IRS components with similar strength may lead to channel frequency selectivity and severe destructive combinations at certain frequencies in wideband systems, which has been omitted in most of the existing studies. Such issues could be mitigated by employing multi-carrier modulation schemes, such as OFDM. Alternatively, the IRS array could be switched on and off adaptively to avoid undesired scenarios. Furthermore, it is found that a closely spaced cluster of IRS elements is more effective than a group of distributed IRS elements. Despite the negative effects of the IRS-induced time delay, the unique channel feature could also be utilised to improve VLC system performance, such as enhancing physical layer security.

Appendix

A. Proof of integration solution

In this appendix, the integral solution in step (a) of the achievable rate derivation (22) is presented. Firstly, the fol-

lowing transformation to the integral can be conducted:

$$\begin{aligned}&\int_0^B \log_2\left(1+A\cos(2\pi f\Delta\tau)\right)\mathrm{d}f\\&\overset{(a)}{=}\frac{1}{2\pi\Delta\tau\ln 2}\int_0^{2\pi\Delta\tau B}\ln\left(1+A\cos(x)\right)\mathrm{d}x\\&\overset{(b)}{=}\sum_{l=1}^{\infty}\frac{(-1)^{l+1}A^l}{2\pi l\Delta\tau\ln 2}\int_0^{2\pi\Delta\tau B}\cos^l x\mathrm{d}x,\end{aligned}\tag{A.1}$$

where A and B are two real and positive numbers. In step (a), the integration variable is changed from f to x. In step (b), the Mercator series is used: $\ln(1+u)=\sum_{l=1}^{\infty}\frac{(-1)^{l+1}u^l}{l}$. The integral of power of a cosine function can be solved by [25]:

$$\begin{aligned}&\int\cos^{2l}x\mathrm{d}x\\&=\frac{1}{2^{2l}}\binom{2l}{l}x+\frac{1}{2^{2l-1}}\sum_{i=0}^{l-1}\binom{2l}{i}\frac{\sin(2l-2i)x}{2l-2i},\end{aligned}\tag{A.2}$$

$$\int\cos^{2l-1}x\mathrm{d}x=\frac{1}{2^{2l-2}}\sum_{i=0}^{l}\binom{2l-1}{i}\frac{\sin(2l-2i-1)x}{2l-2i-1},\tag{A.3}$$

where l can be any positive integers. By using the integral solutions (A.2) and (A.3), the integration solution (A.1) can be further derived as:

$$\begin{aligned}&\int_0^B \log_2\left(1+A\cos(2\pi f\Delta\tau)\right)\mathrm{d}f\\&=\frac{1}{2\pi\Delta\tau\ln 2}\sum_{l_1=1}^{\infty}\frac{(-1)^{2l_1+1}A^{2l_1}}{2l_1}\int_0^{2\pi\Delta\tau B}\cos^{2l_1}x\mathrm{d}x\\&+\frac{(-1)^{2l_1}A^{2l_1-1}}{2l_1-1}\int_0^{2\pi\Delta\tau B}\cos^{2l_1-1}x\mathrm{d}x\\&=\frac{1}{2\pi\Delta\tau\ln 2}\sum_{l_1=1}^{\infty}\frac{(-1)^{2l_1+1}A^{2l_1}}{2l_1 2^{2l_1}}\left(2\pi\Delta\tau B\binom{2l_1}{l_1}\right.\\&\left.+2\sum_{l_2=0}^{l_1-1}\binom{2l_1}{l_2}\frac{\sin\left(2\pi\Delta\tau B(2l_1-2l_2)\right)}{2l_1-2l_2}\right)+\frac{(-1)^{2l_1}A^{2l_1-1}}{(2l_1-1)2^{2(l_1-1)}}\\&\times\left(\sum_{l_2=0}^{l_1-1}\binom{2l_1-1}{l_2}\frac{\sin\left(2\pi\Delta\tau B(2l_1-2l_2-1)\right)}{2l_1-2l_2-1}\right).\end{aligned}\tag{A.4}$$

B. Proof of series convergence

The proof of the series convergence in (22) is provided in this appendix. Since Λ, G_{los} and G_{irs} are positive numbers, the following condition holds:

$$\begin{aligned}&(G_{\mathrm{los}}-G_{\mathrm{irs}})^2+\Lambda^{-1}>0\\&G_{\mathrm{los}}^2+G_{\mathrm{irs}}^2+\Lambda^{-1}>2G_{\mathrm{los}}G_{\mathrm{irs}}\\&\frac{2G_{\mathrm{los}}G_{\mathrm{irs}}}{G_{\mathrm{los}}^2+G_{\mathrm{irs}}^2+\Lambda^{-1}}<1.\end{aligned}\tag{A.5}$$

In step (b) of (A.1), the Mercator series is used, where the convergence condition for Mercator series is $|A\cos(2\pi f\Delta\tau)|<1$. In expression (22), the parameter A is replaced by $\frac{2G_{\mathrm{los}}G_{\mathrm{irs}}}{\Lambda^{-1}+\left(G_{\mathrm{los}}^2+G_{\mathrm{irs}}^2\right)}$. Therefore, the convergence condition for Mercator series is fulfilled in (22).

REFERENCES

[1] X. You, C.-X. Wang, J. Huang, X. Gao, Z. Zhang, M. Wang, Y. Huang, C. Zhang, Y. Jiang, J. Wang *et al.*, "Towards 6G Wireless Communication Networks: Vision, Enabling Technologies, and New Paradigm Shifts," *Science China Information Sciences*, vol. 64, no. 1, pp. 1–74, 2021.

[2] H. Haas, L. Yin, Y. Wang, and C. Chen, "What is LiFi?" *Journal of Lightwave Technology*, vol. 34, no. 6, pp. 1533–1544, 2016.

[3] H. Haas, M. S. Islim, C. Chen, and H. Abumarshoud, *An Introduction to Optical Wireless Mobile Communication*. Artech House, 2021.

[4] Q. Wu, S. Zhang, B. Zheng, C. You, and R. Zhang, "Intelligent Reflecting Surface-Aided Wireless Communications: A Tutorial," *IEEE Transactions on Communications*, vol. 69, no. 5, pp. 3313–3351, 2021.

[5] M. Najafi, V. Jamali, R. Schober, and H. V. Poor, "Physics-based modeling and scalable optimization of large intelligent reflecting surfaces," *IEEE Transactions on Communications*, vol. 69, no. 4, pp. 2673–2691, 2021.

[6] V. Jamali, H. Ajam, M. Najafi, B. Schmauss, R. Schober, and H. V. Poor, "Intelligent Reflecting Surface Assisted Free-Space Optical Communications," *IEEE Communications Magazine*, vol. 59, no. 10, pp. 57–63, 2021.

[7] A. M. Abdelhady, A. K. S. Salem, O. Amin, B. Shihada, and M.-S. Alouini, "Visible Light Communications via Intelligent Reflecting Surfaces: Metasurfaces vs Mirror Arrays," *IEEE Open Journal of the Communications Society*, vol. 2, pp. 1–20, 2021.

[8] H. Abumarshoud, L. Mohjazi, O. A. Dobre, M. Di Renzo, M. A. Imran, and H. Haas, "LiFi through Reconfigurable Intelligent Surfaces: A New Frontier for 6G?" *IEEE Vehicular Technology Magazine*, vol. 17, no. 1, pp. 37–46, 2022.

[9] A. M. Abdelhady, O. Amin, M.-S. Alouini, and B. Shihada, "Revolutionizing optical wireless communications via smart optics," *IEEE Open Journal of the Communications Society*, vol. 3, pp. 654–669, 2022.

[10] M. Jouhari, K. Ibrahimi, H. Tembine, and J. Ben-Othman, "Underwater wireless sensor networks: A survey on enabling technologies, localization protocols, and internet of underwater things," *IEEE Access*, vol. 7, pp. 96 879–96 899, 2019.

[11] J. Kahn and J. Barry, "Wireless Infrared Communications," *Proceedings of the IEEE*, vol. 85, no. 2, pp. 265–298, 1997.

[12] S. Sun, F. Yang, and J. Song, "Sum Rate Maximization for Intelligent Reflecting Surface-Aided Visible Light Communications," *IEEE Communications Letters*, vol. 25, no. 11, pp. 3619–3623, 2021.

[13] H. Abumarshoud, B. Selim, M. Tatipamula, and H. Haas, "Intelligent Reflecting Surfaces for Enhanced NOMA-based Visible Light Communications," in *ICC 2022 - IEEE International Conference on Communications*, 2022, pp. 571–576.

[14] L. Qian, X. Chi, L. Zhao, and A. Chaaban, "Secure Visible Light Communications via Intelligent Reflecting Surfaces," in *ICC 2021 - IEEE International Conference on Communications*, 2021, pp. 1–6.

[15] H. Abumarshoud, C. Chen, I. Tavakkolnia, H. Haas, and M. A. Imran, "Intelligent Reflecting Surfaces for Enhanced Physical Layer Security in NOMA VLC Systems," *arXiv preprint arXiv:2211.09456*, 2022.

[16] Z. Ghassemlooy, W. Popoola, and S. Rajbhandari, *Optical wireless communications: system and channel modelling with Matlab®*. CRC press, 2019.

[17] H. Schulze, "Frequency-domain simulation of the indoor wireless optical communication channel," *IEEE Transactions on Communications*, vol. 64, no. 6, pp. 2551–2562, 2016.

[18] A. M. Abdelhady, O. Amin, A. K. S. Salem, M.-S. Alouini, and B. Shihada, "Channel Characterization of IRS-Based Visible Light Communication Systems," *IEEE Transactions on Communications*, vol. 70, no. 3, pp. 1913–1926, 2022.

[19] A. Nuwanpriya, S.-W. Ho, J. A. Zhang, A. J. Grant, and L. Luo, "PAM-SCFDE for Optical Wireless Communications," *Journal of Lightwave Technology*, vol. 33, no. 14, pp. 2938–2949, 2015.

[20] Y.-P. Lin and S.-M. Phoong, "BER Minimized OFDM Systems with Channel Independent Precoders," *IEEE Transactions on Signal Processing*, vol. 51, no. 9, pp. 2369–2380, 2003.

[21] F. Xiong, *Digital Modulation Techniques*, 2nd ed. Artech House Publishers, 2006.

[22] S. Mardanikorani, X. Deng, and J.-P. M. G. Linnartz, "Sub-carrier loading strategies for dco-ofdm led communication," *IEEE Transactions on Communications*, vol. 68, no. 2, pp. 1101–1117, 2020.

[23] W. Fan, T. B. Cunha, X. Deng, Y. Niu, J. Mo, C. Chen, J.-P. M. G. Linnartz, and G. Zhou, "Achievable rate of mimo-ofdm vlc over low-pass channels," in *2021 IEEE 16th Conference on Industrial Electronics and Applications (ICIEA)*, 2021, pp. 1340–1345.

[24] M. D. Soltani, A. A. Purwita, Z. Zeng, H. Haas, and M. Safari, "Modeling the Random Orientation of Mobile Devices: Measurement, Analysis and LiFi Use Case," *IEEE Transactions on Communications*, vol. 67, no. 3, pp. 2157–2172, 2019.
[25] I. S. Gradshteyn and I. M. Ryzhik, *Table of integrals, series, and products*. Academic press, 2014.

PLACE PHOTO HERE

Cheng Chen received the Ph.D. degree in electrical engineering from The University of Edinburgh, Edinburgh, U.K., in 2017. He is currently employed as a Research Fellow with the Li-Fi Research and Development Centre, University of Strathclyde, where he is working in the fields of visible light communications and LiFi networks. His main research interests include optical wireless communications, visible light communications, and wireless communication for 6G. He has authored or coauthored 40 publications in these areas.

PLACE PHOTO HERE

Shenjie Huang received the B.Sc. degree in optoelectronic engineering from Jiangnan University, China, in 2013, and the M.Sc. degree in signal processing and communications and the Ph.D. degree in electrical engineering from The University of Edinburgh, U.K., in 2014 and 2018, respectively. He is currently a Research Associate with the Institute for Digital Communications, The University of Edinburgh. His main research interest includes optical wireless communications.

PLACE PHOTO HERE

Hanaa Abumarshoud (Senior Member, IEEE) is a Lecturer (Assistant Professor) in the James Watt School of Engineering, the University of Glasgow, Glasgow, UK. Prior to that, she was a Postdoctoral Research Associate at the LiFi Research and Development Centre at the University of Strathclyde (2020-2022) and the University of Edinburgh (2017-2020). She was awarded her MSc and PhD in Electrical and Computer Engineering in 2013 and 2017 from Khalifa University, UAE. She was endorsed as "Global Talent" by the Royal Academy of Engineering in the UK in 2022, and as a "High Level Foreign Talent" by the Chinese Government in 2023. Dr Abumarshoud is a Senior Member of IEEE and an Associate Editor for IEEE Communications letters. She regularly serves as a member of the Technical Program Committee for prestigious conferences and as a technical reviewer for several international journals and conferences within the IEEE, the Royal Society, and the Optical Society. She was recipient of IEEE TAOS Best Paper Award (2022).

PLACE PHOTO HERE

Iman Tavakkolnia (Member, IEEE) is a Chancellor's Fellow (Lecturer) at the Electronic and Electrical Engineering department at the University of Strathclyde. His research focuses on future optical communication systems and lies on the frontier of communication theory, photonic integration, advanced materials, and signal processing. He has participated in several UK and international projects and published more than 40 peer-reviewed papers. He published a pioneering high-impact paper in Nature Light Science and Applications journal in 2021, which demonstrated the simultaneous highspeed communication and efficient energy harvesting using organic solar cells. He is an associate editor of IEEE Communication Letters and has co-chair IEEE WCNC 2023 workshop on Optical Wireless Communication.

PLACE PHOTO HERE

Majid Safari (Senior Member, IEEE) received the B.Sc. degree in electrical and computer engineering from the University of Tehran, Iran, in 2003, the M.Sc. degree in electrical engineering from the Sharif University of Technology, Iran, in 2005, and the Ph.D. degree in electrical and computer engineering from the University of Waterloo, Canada, in 2011. He is currently a Reader at the Institute for Digital Communications, The University of Edinburgh. Before joining Edinburgh in 2013, he was a Post-Doctoral Fellow at McMaster University, Canada. His main research interests include application of information theory and signal processing in optical communications, including fiber-optic communication, free-space optical communication, visible light communication, and quantum communication. He is an Associate Editor of IEEE TRANSACTIONS ON COMMUNICATIONS. He was the TPC Co-Chair of the 4th International Workshop on Optical Wireless Communication in 2015.

PLACE PHOTO HERE

Harald Haas (Fellow, IEEE) received the Ph.D. degree from The University of Edinburgh in 2001. He is currently a Distinguished Professor of mobile communications with The University of Strathclyde/Glasgow and the Director of the LiFi Research and Development Centre. He is the Initiator, the Co-Founder, and the Chief Scientific Officer of pureLiFi Ltd. He has coauthored more than 550 conference papers and journal articles, including articles in science and nature communications. His main research interest includes optical wireless communications. He introduced LiFi to the public at an invited TED Global talk in 2011. Subsequently, LiFi was listed among the 50 best inventions in TIME Magazine in 2011. He gave a second TED Global lecture in 2015 on the use of solar cells as LiFi data detectors and energy harvesters. He is a fellow of IET, the Royal Academy of Engineering, and the Royal Society of Edinburgh. He received the Outstanding Achievement Award from the International Solid State Lighting Alliance in 2016, the IEEE Vehicular Society James Evans Avant Garde Award in 2019, and the Royal Society Wolfson Research Merit Award in 2017.